TÜBİTAK

Turkish Journal of Earth Sciences

http://journals.tubitak.gov.tr/earth/

Research Article

Turkish J Earth Sci
(2014) 23: 513-532

doi:10.3906/yer-1404-11

REE geochemical characteristics of titanium-rich bauxites: the Permian Kanigorgeh horizon, NW Iran

Ali ABEDINI[1,*], Ali Asghar CALAGARI[2]

[1]Department of Geology, Faculty of Sciences, Urmia University, Urmia, Iran
[2]Department of Geology, Faculty of Natural Sciences, Tabriz University, Tabriz, Iran

Received: 20.04.2014 • **Accepted:** 25.07.2014 • **Published Online:** 01.09.2014 • **Printed:** 30.09.2014

Abstract: The Permian Kanigorgeh bauxite horizon is one of the typical titanium-rich bauxite deposits in the northeast of Bukan, West Azerbaijan Province, NW Iran. It is a part of the Irano-Himalayan karst bauxite belt and was developed as discontinuous stratified layers and lenses in Upper Permian carbonates. Mineralogically, diaspore and kaolinite are 2 major mineral phases accompanied by boehmite, smectite, illite, rutile, anatase, hematite, goethite, chlorite, quartz, and plagioclase as minor phases. Geochemical considerations for a selected profile indicate that the concentration values of rare earth elements (REEs) in the bauxite ores range from 8.9 to 200.4 ppm. Eu and Ce anomalies show varying values within the range 0.42–0.65 and 0.12–3.23, respectively. On the basis of Ce behavior, the studied profile can be divided into 2 parts by redox boundary. The most pronounced geochemical characteristics of the studied profile are the occurrences of positive Ce anomalies in the ores of low REE content in the upper part of the profile and negative Ce anomalies in the ores of high REE content in the lower part of the profile. The occurrence of positive and negative Ce anomalies are due to the change of oxidation state of Ce (from Ce^{3+} to Ce^{4+}) in the upper part and the complexing of Ce^{4+} with carbonate ligands in the lower part of the profile. The concordance of the analytical values of Na and Ca with those of Eu revealed that the degree of plagioclase alteration is the most important controlling factor for Eu anomalies in the ores. The obtained results revealed that the variations in the chemistry of weathering solutions (e.g., pH), function of carbonate bedrocks as a geochemical barrier, and discrepancy in degree of stability of lanthanide-bearing primary minerals are the major factors influencing the mobilization, distribution, and fractionation of REEs. The correlation coefficients among elements suggest that Mn-oxides are the principal hosts for REEs in the ores at Kanigorgeh.

Key words: Titanium-rich bauxite, rare earth elements, elemental distribution, Mn-oxides, Kanigorgeh, Iran

1. Introduction

Bauxite deposits are formed by alteration and weathering of parent rocks rich in alumino-silicate minerals. These residual deposits are developed principally in tropical to subtropical climatic conditions with annual rainfall exceeding 1.2 m and an average temperature of >22 °C (Bardossy and Aleva, 1990; Mondillo et al., 2011). According to Bardossy and Combes (1999), these deposits are characterized into 3 major groups: lateritic bauxite deposits, karst bauxite deposits, and Tikhvin-type bauxite deposits. The first group is the product of in situ and direct chemical weathering of alumino-silicate rocks lying beneath the surface. The second group is developed on the surface of more or less karstified carbonates (limestone and dolomite) and scarce marls. The third group is formed on the surface of eroded alumino-silicate rocks and is the erosional product of lateritic bauxite deposits. Bardossy (1982), based upon parameters such as morphology and chemical compositions, classified the bauxite deposits into 6 distinct groups: Mediterranean type, Kazakhstan type, Timan type, Salento type, Tulsk type, and Ariege type. Based upon geographical situations, these deposits occurred in 7 belts throughout the world: the northern Mediterranean coast, Caribbean basin, Urals-Siberia-Central Asia, East Asia, Irano-Himalaya, Southwest Pacific, and North America.

During the last few decades, geochemical investigations proved to have practical applications for determination of various aspects of formation and evolution of bauxite deposits such as the type of parent rocks; the roles of diagenetic, epigenetic, and supergene processes in connection to ore-forming mechanisms; physicochemical conditions of the environment of the ore formation (e.g., pH, Eh, intensity of draining, and climate); the mineral controls on distribution, mobilization, and fractionation of elements [particularly trace and rare earth elements (REEs)] in the course of bauxitization; and tectono-metamorphic evolutions (Özlü, 1983; Mordberg, 1996;

* Correspondence: a.abedini@urmia.ac.ir

MacLean et al., 1997; Öztürk et al., 2002; Temur and Kansun, 2006; Yalcin and Ilhan, 2008, 2013; Esmaeili et al., 2010; Liu et al., 2010, 2012; Mondillo et al., 2011; Aydoğan and Moazzen, 2012; Boni et al., 2012, 2013; Meshram and Randive, 2012; Wei et al., 2013).

There are also many available publications concerning distribution and behavior of major elements, trace elements, and REEs in various profiles of bauxite deposits and/or prospects (e.g., Temur et al., 2005; Temur, 2006; Calagari and Abedini, 2007; Laskou and Economou-Eliopoulos, 2007, 2013; Ma et al., 2007; Mameli et al., 2007; Karadağ et al., 2009; Calagari et al., 2010; Hatipoğlu et al., 2010; Gamaletsos et al., 2011; Hatipoğlu, 2011; Wang et al., 2012; Abedini and Calagari, 2013a, 2013b, 2013c; Gu et al., 2013; Hanilçi, 2013; Li et al., 2013; Liu et al., 2013; Wang et al., 2013; Wei et al., 2013; Zhang et al., 2013; Babechuk et al., 2014; Giorgis et al., 2014; Mongelli et al., 2014). The results of these investigations show that consideration of factors controlling the distribution and behavior of REEs during bauxitization processes is one of more interesting geochemical subjects for further research works.

Based upon the world's geographical distribution of bauxite deposits (Bardossy, 1982), the bauxite deposits in Iran belong to the Irano-Himalayan karst bauxite belt. They are mostly similar to Mediterranean-type karst bauxites (Calagari and Abedini, 2007; Abedini and Calagari, 2013a, 2013b, 2013c). Northwestern Iran is one of the important bauxite-bearing regions along the Irano-Himalayan karst bauxite belt. In this region, the bauxite deposits were temporally developed in 4 periods: the Permian, Permo-Triassic, Triassic, and Triassic-Jurassic. The Kanigorgeh area in the northwest of Iran contains 2 bauxite-bearing horizons of Permian and Permo-Triassic ages. The development of the titanium-rich bauxite ores and the formation of the ferruginous bauxite ores are the most outstanding characteristics of the Permian and Permo-Triassic horizons, respectively. Geological, mineralogical, and geochemical characteristics of the ferruginous bauxite ores in the Permo-Triassic horizon were investigated in detail by Abedini and Calagari (2013b). No geochemical studies, however, on Permian Ti-rich bauxite horizon have been undertaken so far. It seems that geochemical studies on these extraordinary and unique ores can contribute to the exploration and identification of new high-Ti content bauxite prospects in other parts of the Irano-Himalayan karst bauxite belt in particular, as well as in other bauxite belts in general. To achieve this goal, we have endeavored in our research to conduct field observations as well as petrographic, mineralogical, and geochemical investigations to consider the factors affecting the distribution, mobilization, and fractionation of REEs and the potential causes of Eu and Ce anomalies in the Ti-rich bauxite ores in the Kanigorgeh area.

2. Geological setting

Consideration of regional geology in northwestern Iran shows that there is good and distinct coexistence between Permian carbonate rocks and bauxitic-lateritic deposits in the Bukan and Mahabad districts. Geological features of these districts are shown in Figure 1. Five residual deposits in relation with Permian carbonates have been recognized in the Bukan and Mahabad districts so far. The residual deposits in the Mahabad district (Sheikh-Marut and Hossein-Abad) have chiefly lateritic composition, while the Bukan district (Kanigorgeh, Kanisheeteh, and Shahindezh) possess mainly bauxitic composition. The locations of these deposits are also shown in Figure 2.

The Kanigorgeh area is located about 20 km northeast of Bukan, West Azerbaijan Province, NW Iran. Based upon classification of structural domains of Iran (Nabavi, 1976), the area is a part of the Khoy-Mahabad structural zone (Figure 1). The characteristics of regional geology of the bauxite deposits in this area were explained in detail by Kamineni and Efthekhar-Nezad (1977) and Abedini and Calagari (2013b). The oldest lithologic units in this area are sandstone and shale of the Dorud Formation (Lower Permian), which are overlain by carbonates (limestone and dolomite) of the Ruteh Formation (Upper Permian) and dolomitic rocks of the Elika Formation (Triassic). The latter is covered by a series of arenaceous-argillaceous (sandstone, shale, and conglomerate) and carbonate rocks of Cretaceous age. The above sequence is overlain by Miocene limestone (Qom Formation) and Quaternary alluvial sediments (Figure 3).

Depositional cessation during Permian and Permo-Triassic times brought about the development of 2 distinct bauxitic horizons in this area. The Permian bauxitic horizon consists of 4 discontinuous stratified layers and/or lenses and has a sharp boundary with the enclosing carbonates (limestone and dolomite) of the Ruteh Formation. This horizon extends over 1 km and has varying thicknesses (2–11 m) and trends (N-S, NE-SW, and NW-SE) (Figure 3). The host rocks contain plenty of calcite microveinlets and cherty bands and nodules. The bauxitic horizon of the Permo-Triassic relative to that of the Permian is more widespread and consists of 8 discontinuous stratified layers and lenses. This horizon runs lengthwise over 3.2 km and has varying thicknesses (5–17 m). Lithostratigraphically, this horizon is developed along the contact of the Upper Permian carbonates (Ruteh Formation) and Triassic dolomite (Elika Formation) and has varying trends (N-S and NW-SE) (Figure 3). Both horizons along with their enclosing rocks were severely folded (Abedini and Calagari, 2013b). The Permian horizon is thicker in karstic sinkholes and depressions than in the high lands. Locally, the Permian horizon is cut and becomes offset (~50 m) by strike-slip and thrust faults (see Figure 3), resulting in the development of a cataclastic texture within the ores.

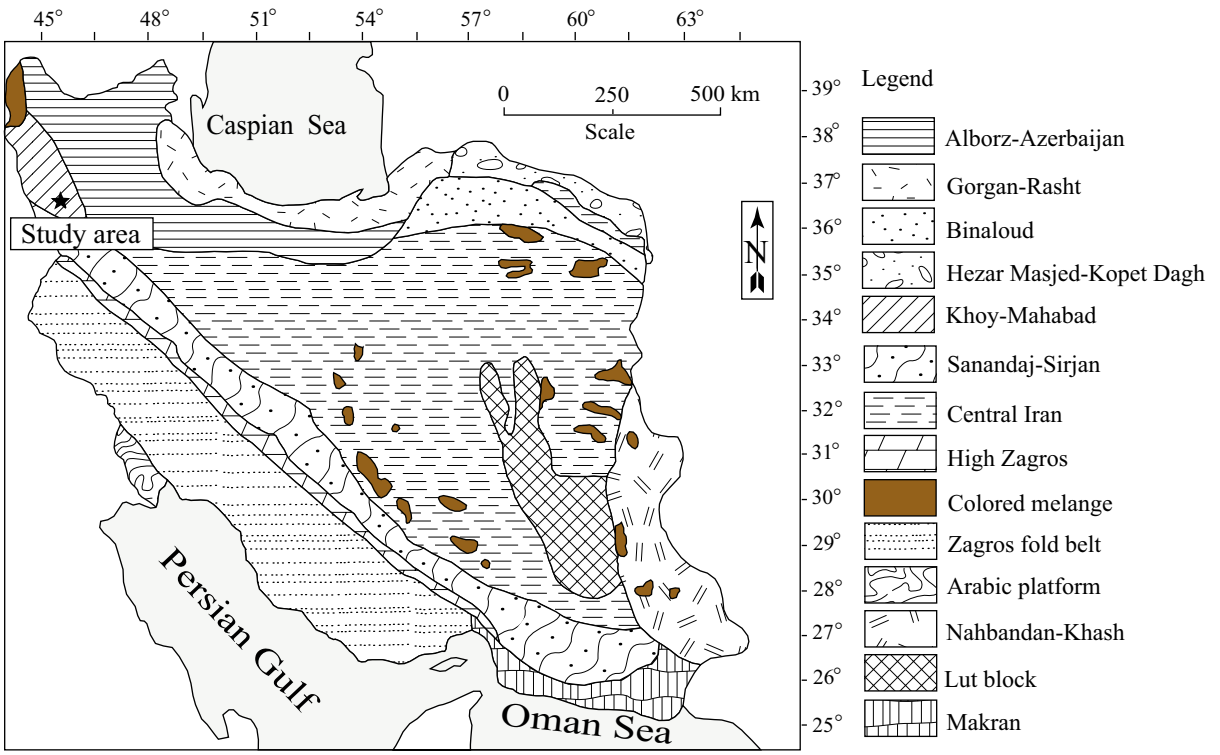

Figure 1. A simplified regional geotectonic map of Iran (Nabavi, 1976) showing major geological-structural zones. Location of studied area is marked by asterisk.

On the basis of color, 3 types of ores were recognized in the Permian horizon, which are, from top toward the bottom, greenish gray, dark green, and red to brownish red (Figure 4). The common characteristics of all these types of ores is the development of manganese dendrites on the rock surface. Limonitization, development of ferruginous nodules, and hematite microveinlets are the most important mesoscopic characteristics of the red and brownish red ores. The dark gray and greenish gray ores are characterized by soapy feel, conchoidal fracture surfaces, and presence of spherical features in an aphanitic matrix.

3. Sampling and laboratory methods

3.1. Sampling

In this study, a profile perpendicular to the strike of bauxitic layers was selected (see Figure 3) and 20 systematic and representative samples with varying intervals (25–80 cm) were collected (see Figure 4) from an exploratory pit. Of these, 8 samples belonged to the greenish gray ores, 4 to the dark green ores, and 8 to the red and brownish red ores.

3.2. Mineralogical analyses

Laboratory works began with preparation of thin and polished sections from all 20 samples and their examination under microscope. For determination of the major rock-forming minerals in the ores, 8 samples were randomly selected for X-ray diffraction (XRD) analysis using a SIEMENS model D-5000 diffractometer with CuKα radiation, graphite monochromator, voltage 40 kV, beam current 80 mA, continuous scanning, scanning speed 8°/min, scan range 2°–70°, slit DS = SS = 1°, ambient temperature 18 °C, and humidity 30% in the facilities of the Geological Survey of Iran.

3.3. Chemical analyses

Whole-rock samples were crushed to 200-mesh size particles using an agate mill. All 20 samples were prepared for chemical analyses in the laboratories of ALS Chemex, Canada. Quantitative values of major and minor elements, trace elements, and REEs were determined by using inductively coupled plasma-atomic emission spectrometry and inductively coupled plasma-mass spectrometry analyzing methods, respectively. Loss on ignition (LOI) values were determined by weight loss of a 1-g sample after heating at 950 °C for 90 min. Detection limits were for major elements and LOI 0.01%: for Cr, 10 ppm; for V, Ni, and Cu, 5 ppm; for Co, Y, Ba, Tl, La, and Ce, 0.5 ppm; for Nb, Rb, and Hf, 0.2 ppm; for Sr, Ta, Ga, Nd, and Lu, 0.1 ppm; for Cs, Tb, Ho, and Tm, 0.01 ppm; for Th, 0.04; for U, Gd, and Dy, 0.05 ppm; for Zr, 2 ppm; and for Pr, Sm, Eu, Er, and Yb,

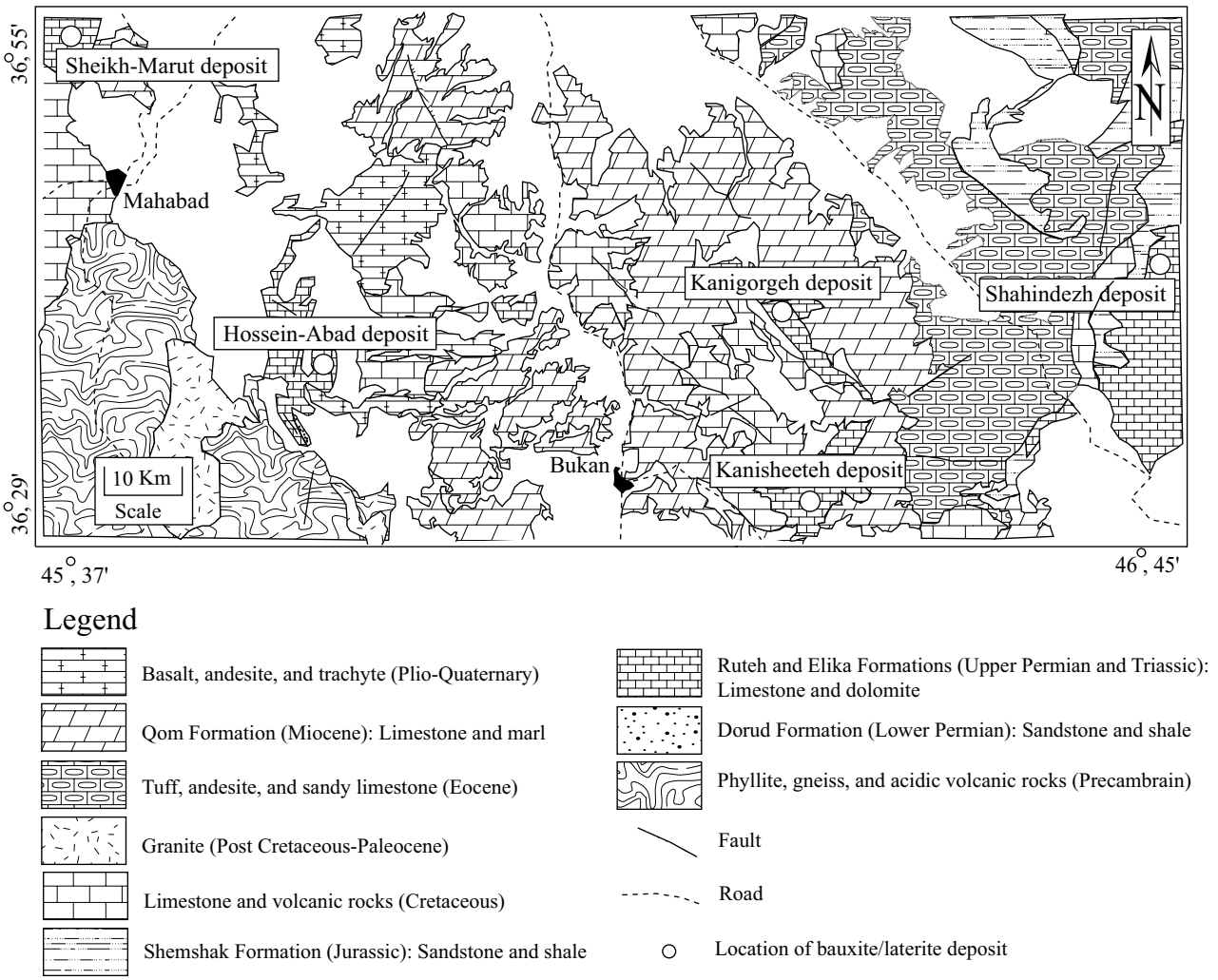

Figure 2. Geological map (modified and compiled from Efthekhar-Nezad 1973; Alvai-Naeini et al., 1976) showing the locations of some studied bauxite/laterite deposits in northwestern Iran.

0.03 ppm. Furthermore, for determining the relationship between elements in the selected bauxitic profile, attempts were made to calculate the Pearson correlation coefficients among selected elements by using SPSS 16.

4. Results

4.1. Mineralogy and texture

Because they were fine-grained, identification of minerals in the bauxite ores under a microscope was not possible. Therefore, petrographic examinations were principally focused on textural features of the ores. Based on these studies, spherical and dumbbell-shaped features along with a microgranular and pelitomorphic matrix are the major texture-forming components in the ores (Figures 5a–5f). The spherical grains are often ooids and pisoids, whose presence within the ores testifies to the original heterogeneity of colloids that resulted from alteration and weathering of parent rocks. The various shapes and sizes of ooids and pisoids along with elongate and oblate nodules indicate redepositional conditions during the evolution of this deposit. The fractures within the spherical components of the ores are observable in 2 different forms. Some are in radial and irregular shapes and are often limited to within a component (Figure 5a), while some others cross the border of components and extend into the matrix of the ores. The presence of both types of fractures indicates contraction of gels during the ore formation and the subsequent effects of epigenetic processes on the ores. Hematite is the most important identifiable nucleus in the spherical component (Figure 5f). The presence of hematite microveinlets within the matrix testifies to the redistribution of iron in the weathered profile. Considering the mode of distribution of texture-forming components and matrix, various kinds of textures such as pelitomorphic, microgranular, ooidic,

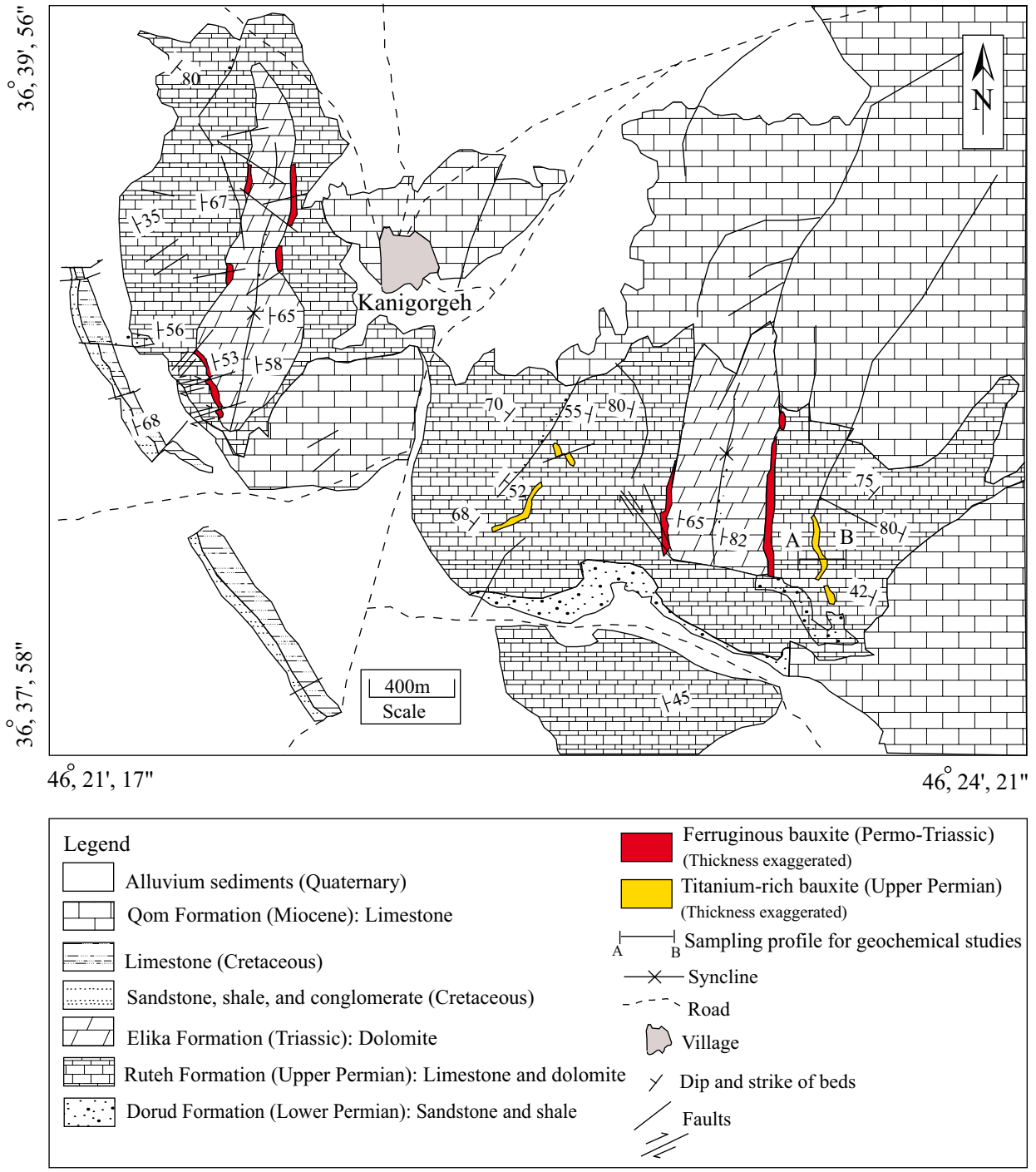

Figure 3. Geological map of the study area (after Abedini and Calagari, 2013b) showing the position of discontinuous layers of the titanium-rich bauxite ores at Kanigorgeh.

pisoidic (Figure 5b), nodular, and collomorphic-fluidal (Figure 5e) developed within the ores.

The XRD analyses show that diaspore is the main mineral phase of the ores (Table 1; Figure 6). Kaolinite is present both as a major mineral phase in certain ores and as minor in some others. Minerals such as boehmite, smectite, illite, rutile, anatase, hematite, goethite, chlorite, quartz, and plagioclase occurred as minor mineral phases in the ores (Table 1; Figure 6).

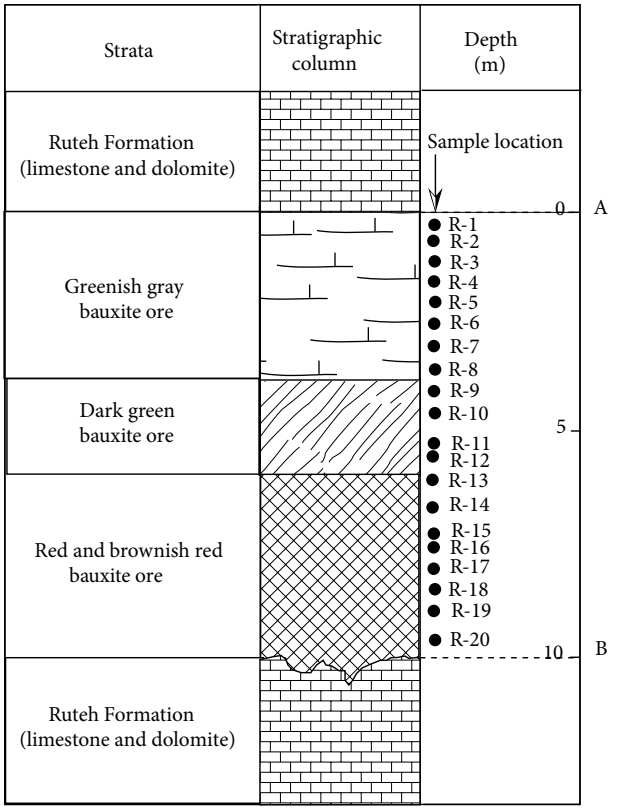

Figure 4. Stratigraphic column across a selected profile of the Permian bauxite horizon at Kanigorgeh (for position, see Figure 3) with indication of analyzed samples.

4.2. Geochemistry

The analytical values of major, minor, trace, and rare earth elements in 20 ore samples collected from the studied profile are listed in Table 2.

The distribution pattern of major and minor elements normalized to upper continental crust (UCC) (Rudnick and Gao, 2004) illustrates that with increasing concentration values of Al, Ti, Mn, and P, the values of Na, K, Ca, and Mg decrease. Iron, however, displays dual (decrease-increase) behavior during the progression of bauxitization processes (Figure 7). Bivariate plots among oxides demonstrates that there exist good and strong correlations between pairs of Al_2O_3–TiO_2 (Figure 8a) and SiO_2–K_2O (Figure 8b) and negative correlations between pairs of Al_2O_3–Fe_2O_3 (Figure 8c) and TiO_2–Fe_2O_3 (Figure 8d) in the studied ores.

The correlation coefficients between pairs of Al_2O_3–TiO_2 (r = 0.95), SiO_2–CaO (r = 0.91), and SiO_2–K_2O (r = 0.77) are strongly positive, while between pairs of Al_2O_3–Fe_2O_3 (r = – 0.89) and TiO_2–Fe_2O_3 (r = –0.78) they are strongly negative. Using ternary plots of Al_2O_3–Fe_2O_3–SiO_2 (Schellamnn, 1986; Beavais, 1991; Aleva, 1994) unveils some important points concerning the chemical characteristics of the bauxite ores. The Kanigorgeh data points on these plots show that the ores have bauxite to kaolinitic bauxite compositions (Figure 9) and formed during moderate lateritization processes (Figure 10). Deferrugenization was the only important controlling mechanism during the evolution of the ores (Figure 11).

Comparison of the mean chemical composition of certain selective oxides and REEs in the Permian bauxite ores at Kanigorgeh with those of some known bauxitic-lateritic deposits in the world (Iran, Turkey, India, Greece, Venezuela, Madagascar, and Italy) (Table 3) reveals that despite the low values of REEs, the ores at Kanigorgeh possess high contents of TiO_2 and MnO relative to most well-known bauxitic-lateritic deposits in the world.

The distribution pattern of trace elements normalized to the UCC (Rudnick and Gao, 2004) reveals that, parallel to the increase of concentration values of V, Cr, Co, Ga, Zr, Nb, Mo, Hf, Ta, W, and Tl, the values of Ni, Cu, Zn, Rb, Y, Cs, and Pb decrease. However, Sn, U, and Th depict 2 trends of increase and decrease in the course of evolution of the ores (Figure 7). Bivariate plots among trace elements and certain minor oxides exhibit other interesting geochemical aspects of the ores. Shown on these bivariate diagrams are the positive and strong correlations between pairs of K_2O–Rb, K_2O–Cs, K_2O–Ba, and K_2O–Sr (Figures 8e–8h); pairs of Fe_2O_3–U, Fe_2O_3–Th, and Fe_2O_3–Co (Figures 8i–8k); and pairs of MnO–Mo, MnO–Ni, MnO–Zn, and MnO–Tl (Figures 8l–8o).

Distribution patterns of REEs normalized to the UCC (Rudnick and Gao, 2004) indicate various degrees of depletion of these elements relative to the UCC in most studied samples (Figure 7). According to the results of chemical analyses, the anomalous levels of REEs in the bauxite ores are $\Sigma REE_{La\text{-}Lu}$ = 8.91–200.38 ppm, $\Sigma LREE_{La\text{-}Nd}$ = 7.63–167.46 ppm, $\Sigma MREE_{Sm\text{-}Ho}$ = 0.95–25.53 ppm, $\Sigma HREE_{Er\text{-}Lu}$ = 0.33–9.71 ppm, and La/Y = 0.09–6.11 (Table 4). The calculation of Eu and Ce anomalies obtained from the following equations (Taylor and McLennan, 1985) shows that the anomaly values have ranges of 0.42–0.65 and 0.21–3.23, respectively (Table 4):

$Eu/Eu^* = Eu_N / (\sqrt{Sm_N \times Gd_N})$,

$Ce/Ce^* = 2Ce_N / (La_N + Pr_N)$,

where N stands for the normalization of REEs to chondrite.

5. Discussion

5.1. Mobilization, distribution, and fractionation of REE in the bauxite profile

Plotting of concentration variations of light REEs (LREEs; La–Nb), middle REEs (MREEs; Sm–Ho), heavy REEs (HREEs; Er–Lu), and REEs (La–Lu) of the ore samples against depth in the studied profile elucidates 2 important points for distribution of REEs (Figures 12a–12d): the distribution patterns of LREEs, MREEs, HREEs, and

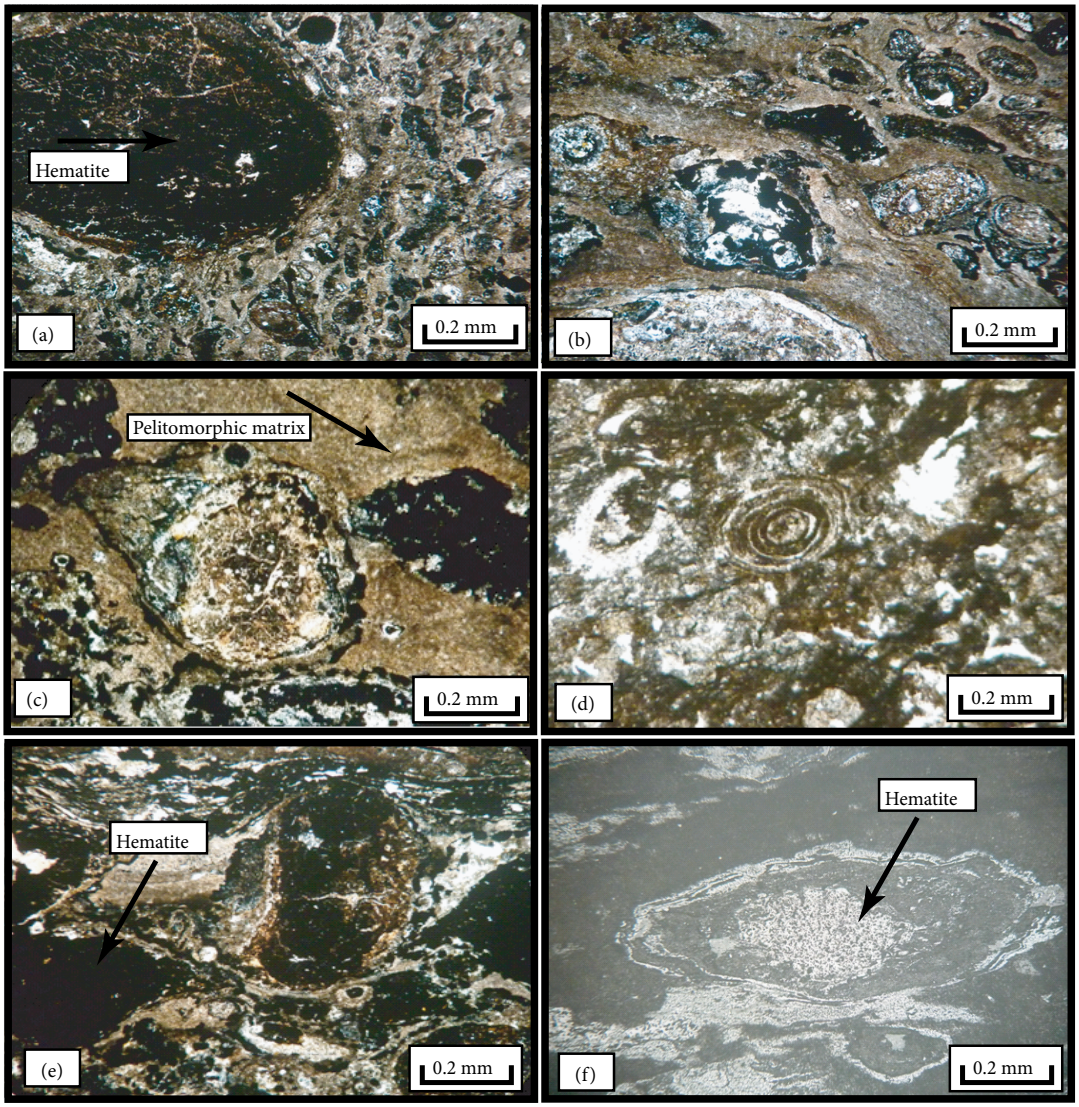

Figure 5. Photomicrographs of some bauxite ores at Kanigorgeh. **(a)** Spherical features (ooids and pisoids) (XPL). **(b)** Ooids and pisoids with various shapes and sizes (XPL). **(c)** Dumbbell-shaped pisoids (formed by epigenetic processes) set in a pelitomorphic matrix (XPL). **(d)** A pisoid (at center) with conspicuous concentric bands (XPL). **(e)** Collomorphic-fluidal texture (XPL). **(f)** Elliptical and dumbbell-shaped hematite in an aphanitic matrix (polarized reflective light).

Table 1. Constituent minerals (identified by XRD analyses) in the bauxite ores at Kanigorgeh.

Sample no.	Minerals identified	
	Major	Minor
R-1	Diaspore, kaolinite	Rutile, anatase, illite, quartz, boehmite
R-4	Diaspore, kaolinite	Smectite, illite, rutile, chlorite
R-7	Diaspore, kaolinite	Boehmite, smectite, hematite, anatase, kaolinite
R-10	Diaspore, kaolinite	Kaolinite, rutile, anatase, hematite, goethite,
R-12	Diaspore	Boehmite, kaolinite, illite, goethite, hematite, rutile, anatase, smectite, quartz
R-16	Diaspore	Boehmite, kaolinite, illite, goethite, hematite, rutile, anatase, smectite, chlorite, plagioclase
R-18	Diaspore	Kaolinite, goethite, hematite, rutile,
R-20	Diaspore	Kaolinite, illite, hematite, rutile, anatase,

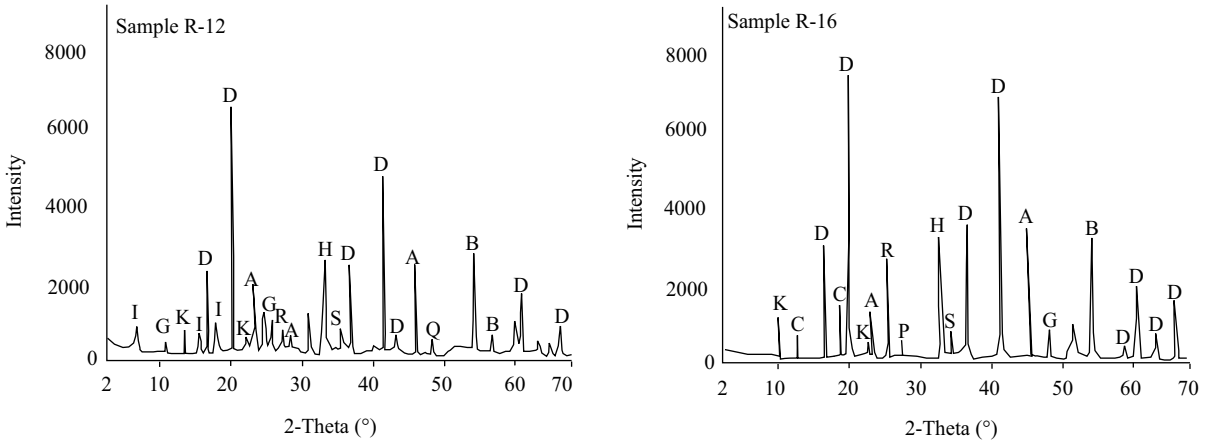

Figure 6. XRD analyses for the 2 typical bauxite ores at Kanigorgeh. D: Diaspore; I: illite; G: goethite; K: kaolinite; A: anatase; R: rutile; B: boehmite; Q: quartz; S: smectite; P: plagioclase; C: chlorite; H: hematite.

REEs in the upper and middle parts of the profile exhibit irregular and zigzag shapes, and they show elevated values in the lower parts. In this study, for interpretation of causes of REE variations in the sampled profile, attempts have been made to calculate the La/Y values in the ores. La/Y proved to be a suitable parameter for determination of pH in the environment of ore formation, so values of <1 and >1 are indicative of acidic and alkali environments, respectively (Crinci and Jurkowic, 1990). This ratio at Kanigorgeh ranges from 0.09 to 6.11. The environment of ore formation from the surface to a depth of about 6.5 m had chiefly acidic conditions, but it gradually changed to basic toward deeper parts (6.5–10 m) (Figure 13). The prevalence of acidic conditions in the upper and middle parts of the profile and basic in the lower parts led us to infer that the percolating acidic solutions caused the leaching of REEs from the upper and middle parts and then their deposition (due to the buffering of weathering solutions near the carbonate bedrocks) in the lower parts. In fact, this mechanism brought about redistribution and hence concentration of REEs in the lower parts of the profile. It seems that the main effective factor for irregular distribution of REEs in the upper and middle parts of the profile was the discrepancy in the degree of resistance of the primary REE-bearing minerals against meteoric percolating solutions. Furthermore, according to the high similarity of the concentration trends of LREEs, MREEs, and HREEs, it can further be deduced that the REEs as a whole did not experience a considerable fractionation after deposition of ores into karstic holes at Kanigorgeh.

In this study, for quantitative consideration of the fractionation degrees between REEs, various ratios of REEs like La_N/Yb_N, La_N/Sm_N, and Gd_N/Yb_N were used. La_N/Yb_N establishes the degree of fractionation of LREEs from HREEs during geochemical processes (Aubert et al., 2001; Yusoff et al., 2013), while the other 2 ratios determine the degree of fractionation between LREEs and MREEs and between MREEs and HREEs (Yusoff et al., 2013). The values of those ratios have ranges of La_N/Yb_N = 0.44–1.85, La_N/Sm_N = 0.80–5.15, and Gd_N/Yb_N = 0.14–3.18 (Table 4), which are indicative of relatively weak fractionations between LREEs and MREEs as well as HREEs during bauxitization. Moreover, the distribution pattern of REEs normalized to chondrite (Taylor and McLennan, 1985) also demonstrates weak fractionations of REEs along with occurrence of both positive and negative anomalies for Ce and negative anomalies for Eu (Figure 14). The correlation coefficients among REEs show varying ranges of 0.75–0.99 (among La to Nd), 0.81–0.99 (among Sm to Ho), and 0.97–0.99 (among Er to Lu) (see Table 5). The deduction can be made from data in Table 5 that HREEs have the stronger intrinsic correlations among themselves relative to MREEs and LREEs. These explanations demonstrate that the fractionations among LREEs and MREEs were greater than those of HREEs in Kanigorgeh Ti-rich bauxite ores.

5.2. Controlling factors on Ce and Eu anomalies

The values of Ce anomalies have a range of 0.21–3.23. Plotting of the Ce anomalies against depth shows that these values are positive from the surface up to a depth of ~6.5 m and then gradually become considerably negative in the deeper parts (Figure 15a). The studied ores, on the basis of REE values and Ce anomalies, can be divided into 2 distinct parts. Those in the upper part (from the surface to a depth of ~6.5 m) that is actually a leached zone contain positive Ce anomalies (1.62–3.23) with low values of REEs (8.91–133.98 ppm) (Figure 16). The lower part that lies beneath the leached zone is in fact an enrichment zone and has negative Ce anomalies (0.24–0.61) and high REE values (151.04–200.38 ppm) (Figures 12a and 13). In view of concentration trends

Table 2. Results of chemical analyses for major, minor, trace, and rare earth elements in the studied bauxite ores at Kanigorgeh.

	Detection limit	R-1	R-2	R-3	R-4	R-5	R-6	R-7	R-8	R-9	R-10	R-11	R-12	R-13	R-14	R-15	R-16	R-17	R-18	R-19	R-20
SiO_2 (wt.%)	0.01	21.25	23.60	21.25	22.7	23.43	25.62	22.41	21.95	28.55	19.6	24.60	23.55	20.81	16.25	20.30	22.40	18.90	26.07	21.80	20.35
Al_2O_3	0.01	54.20	51.80	54.2	52.80	50.67	47.15	50.42	51.02	41.5	48.84	43.70	46.64	45.12	46.465	41.08	50.42	56.6	46.65	54.32	55.40
Fe_2O_3	0.01	0.73	0.80	1.30	0.8	3.71	6.13	5.72	5.70	11.45	10.74	12.05	10.71	14.12	15.04	20.82	6.01	0.65	6.13	0.60	0.69
CaO	0.01	0.43	0.45	0.63	0.52	0.61	0.57	0.50	0.52	0.57	0.52	0.63	0.55	0.50	0.64	0.52	0.54	0.45	0.41	0.44	0.55
MgO	0.01	0.15	0.19	0.15	0.19	0.19	0.18	0.18	0.16	0.23	0.15	0.19	0.17	0.14	0.12	0.14	0.17	0.16	0.22	0.21	0.17
Na_2O	0.01	0.36	0.37	0.52	0.41	0.56	0.49	0.41	0.42	0.48	0.47	0.52	0.49	0.42	0.58	0.46	0.45	0.38	0.39	0.42	0.47
K_2O	0.01	0.32	0.41	0.35	0.33	0.38	0.41	0.35	0.32	0.45	0.35	0.35	0.39	0.35	0.21	0.30	0.39	0.26	0.49	0.49	0.34
TiO_2	0.01	9.96	9.6	9.45	9.6	7.88	7.32	8.56	8.65	5.05	8.23	5.7	7.17	6.87	8.41	6.15	8.31	10.32	7.32	9.21	10.14
MnO	0.01	0.70	0.39	0.22	0.43	0.31	0.20	0.52	0.39	0.46	0.57	0.20	0.35	0.43	0.48	1.04	1.20	1.12	0.96	0.99	1.01
P_2O_5	0.01	0.26	0.28	0.26	0.28	0.28	0.30	0.28	0.26	0.33	0.25	0.30	0.27	0.26	0.20	0.22	0.25	0.23	0.31	0.33	0.26
LOI	0.01	11.61	12.08	11.61	11.74	11.32	11.55	10.58	10.52	10.87	10.24	11.74	9.68	10.95	11.52	8.95	9.81	10.88	11.03	11.17	10.58
Sum	-	99.97	99.97	99.94	99.80	99.34	99.93	99.93	99.91	99.94	99.96	99.98	99.97	99.97	99.92	99.98	99.95	99.95	99.98	99.98	99.96
V (ppm)	5	572	558	522	525	451	380	472	450	372	566	416	392	540	580	374	447	686	415	497	521
Cr	10	90	510	360	410	450	740	690	690	1370	1290	1470	1290	1700	1810	2100	720	480	740	390	490
Co	0.5	36.3	100.2	64.3	20.0	102.3	306.3	285.9	240.0	410.2	536.8	500.0	410.3	287.4	654.2	541.0	180.2	32.5	210.2	30.0	34.4
Ni	5	68	37	13	42	12	11	35	35	48	56	17	26	40	47	104	119	108	96	98	100
Rb	0.2	19.2	29.5	19.2	24.2	31.3	20.1	25.9	23.3	32.7	7.1	7.1	32.7	16.2	6.5	5.4	25.9	8.8	41.1	60.0	14.0
Cs	0.01	3.27	4.06	3.47	3.27	3.76	4.06	3.47	3.17	4.46	3.47	3.47	3.86	3.62	2.14	3.01	3.91	2.63	4.78	4.92	3.35
Ba	0.5	32.6	41.2	35.7	33.7	38.8	40.2	35.7	32.6	42.1	35.7	35.7	37.4	35.7	20.6	30.6	39.8	26.5	48.2	49.5	34.7
Sr	0.1	33.6	37.4	32.4	35.1	35.2	36.1	33.6	33.8	37.8	31.5	36.1	35.1	32.5	24.5	27.1	30.2	29.8	39.4	36.1	30.2
Ga	0.1	48.0	41.2	48.0	43.2	41.3	34.7	43.6	46.7	37.5	48.4	38.4	39.2	30.5	39.2	36.1	43.6	60.6	37.3	46.3	54.3
Th	0.04	7.49	8.85	7.49	5.23	8.81	10.15	11.28	11.93	15.07	15.37	15.37	15.07	14.47	14.41	20.62	11.28	10.12	9.96	9.51	8.80
U	0.05	2.39	1.92	2.39	1.25	2.47	2.57	3.14	3.25	3.89	4.49	4.49	3.89	5.69	5.36	6.12	3.14	2.85	2.90	1.65	2.62
Cu	5	17	9	5	9	7	5	12	9	8	14	5	8	10	12	25	31	27	22	21	23
Y	0.5	13.7	12.9	13.5	14.4	12.9	10.9	10.8	12.9	9.3	10.1	9.8	9.1	9.5	11.8	8.9	11.1	13.7	10.5	12.2	14.2
Zr	2	1248	1237	1248	1299	1157	1066	1041	1043	833	905	905	833	910	1079	751	1041	1259	1035	1115	1254
Ta	0.1	4.7	4.5	4.9	4.8	4.6	4.3	4.6	4.2	3.8	4.4	4.0	4.2	3.9	4.1	3.7	4.5	5.1	4.2	4.9	5.0
Mo	2	19	15	12	17	23	9	18	12	16	19	13	12	14	13	51	50	48	45	46	50
Zn	5	19	17	7	15	10	6	18	14	13	14	12	9	17	17	19	25	24	23	23	25
Tl	0.5	3.5	1.5	2	1	1	1.5	2	2.5	2	1.5	2	1.5	2	3	3	4	4	4	4.5	3.5

Table 2. (Continued).

W	1	7	3	4	16	2	3	4	5	4	3	4	3	10	6	6	8	17	8	9	7
Sn	1	2	4	1	1	1	1	1	2	1	1	2	1	1	2	2	2	7	2	3	9
Pb	5	8	6	6	6	6	6	7	6	6	7	6	6	6	7	9	9	9	9	8	10
Nb	0.2	31.9	30.7	30.2	29.8	25.2	23.4	26.5	27.7	16.2	26.4	18.2	23.0	22.0	26.9	18.7	26.6	32.1	23.4	29.5	31.7
Hf	0.2	22.3	35.2	36.8	20.9	32.5	16.4	18.6	35.4	28.7	18.4	12.8	31.9	15.4	32.7	13.1	18.6	38.2	16.4	37.4	22.2
La (ppm)	0.5	14.32	14.55	2.62	4.95	6.11	1.75	10.91	4.95	2.33	7.28	0.87	3.25	10.91	12.51	54.42	50.88	47.34	47.34	45.30	42.60
Ce	0.5	67.24	62.13	13.86	22.45	84.63	10.22	36.78	22.56	18.45	30.56	5.52	19.45	48.56	51.36	35.14	64.12	60.25	20.87	23.24	40.21
Pr	0.03	3.15	2.78	0.49	1.61	1.25	0.33	2.75	1.61	0.84	2.72	0.17	0.87	2.75	2.47	11.73	11.48	11.22	11.22	10.62	10.10
Nd	0.1	26.63	11.83	1.46	7.28	4.07	1.26	12.46	7.28	5.63	13.10	1.07	2.76	12.46	10.67	40.55	40.98	41.42	41.42	41.13	37.28
Sm	0.03	5.10	1.98	0.33	2.54	1.18	0.24	3.37	2.54	1.81	4.75	0.15	0.76	3.37	1.86	6.61	7.41	8.22	8.22	7.41	7.39
Eu	0.03	0.70	0.34	0.08	0.58	0.27	0.06	0.71	0.58	0.38	1.08	0.04	0.17	0.71	0.32	1.13	1.22	1.06	1.06	1.03	0.96
Gd	0.05	4.80	2.90	0.60	4.81	1.57	0.45	5.96	4.81	2.37	9.01	0.29	1.09	5.96	1.14	6.90	6.80	6.70	6.70	6.37	4.03
Tb	0.01	0.76	0.47	0.07	0.73	0.20	0.05	0.93	0.73	0.32	1.39	0.04	0.14	0.93	0.29	1.08	1.07	1.06	1.06	1.01	0.95
Dy	0.05	4.69	3.45	0.57	4.20	1.32	0.47	5.65	4.20	1.98	7.84	0.36	0.95	5.65	1.56	6.91	6.42	5.93	5.93	6.02	5.33
Ho	0.01	0.90	0.58	0.15	0.80	0.20	0.11	1.02	0.80	0.31	1.46	0.07	0.17	1.02	0.34	1.32	1.27	1.21	1.21	1.20	1.09
Er	0.03	2.60	1.79	0.35	1.51	0.44	0.24	2.23	1.51	0.99	2.67	0.13	0.39	2.23	0.90	4.25	3.83	3.41	3.41	3.49	3.07
Tm	0.01	0.39	0.24	0.02	0.16	0.09	0.02	0.28	0.16	0.10	0.31	0.03	0.05	0.28	0.14	0.64	0.59	0.54	0.54	0.50	0.49
Yb	0.03	2.32	1.34	0.24	0.84	0.43	0.19	1.39	0.84	0.57	1.45	0.15	0.33	1.39	0.73	4.24	3.77	3.31	3.31	3.23	2.98
Lu	0.01	0.38	0.26	0.02	0.12	0.10	0.02	0.24	0.12	0.12	0.22	0.02	0.06	0.24	0.12	0.58	0.54	0.50	0.50	0.49	0.45

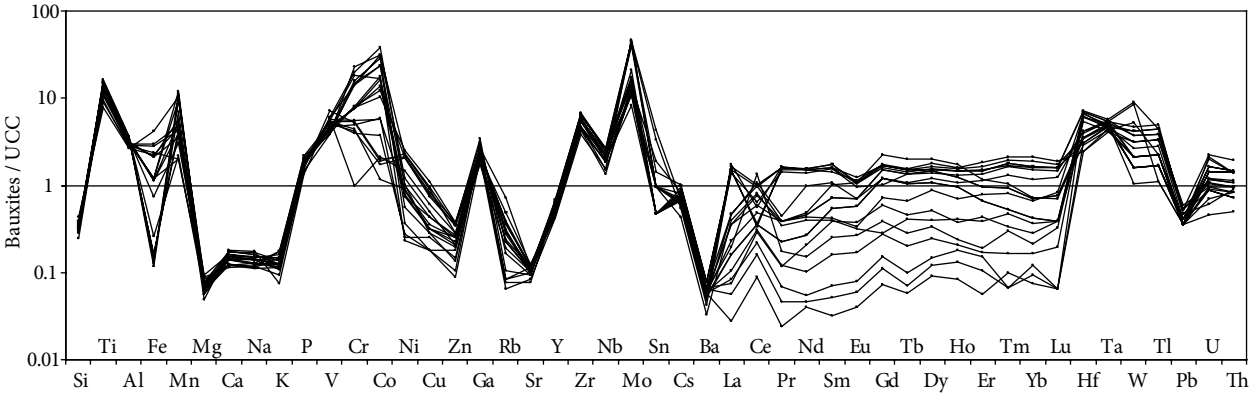

Figure 7. Distribution pattern of some major, minor, trace, and rare earth elements of ore samples normalized to the UCC in the Permian bauxite horizon at Kanigorgeh.

of REEs and their relations with Ce anomalies, the ores at Kanigorgeh have high similarity to the mineralization of REEs in Thailand (at Phuket) (Sanematsu et al., 2013) and southern China (Bao and Zhao, 2008; Chi and Tian, 2009). Although concentration values of REEs in the ores at Kanigorgeh are less than those of these 2 areas, the positive anomalies of Ce in the upper parts of the profile at Kanigorgeh indicate that Ce was fixed as Ce^{4+} under acidic and oxidizing conditions. Noting the prevalence of alkaline conditions in the lower parts of the profile (Figure 13), the only logical and acceptable factor for the generating of negative anomalies for Ce in the lower part of the profile is coupled complexation of Ce^{4+} with carbonate ligands and its leaching during bauxitization processes (Karadağ et al., 2009). The Eu anomaly values range from 0.42 to 0.56 (Table 4). This relatively narrow range may act as conservative index during bauxitization processes (Figure 15b). By considering the good and positive correlation between Eu/Eu* and CaO (r = 0.97) (Figure 17a) and between Eu/Eu* and Na_2O (r = 0.96) (Figure 17b), it can be inferred that the degree of plagioclase alteration was the important controlling factor for the minor variation in Eu anomalies in the ores at Kanigorgeh.

5.3. Mineral controls on the REE distribution

The secondary minerals like phosphates along with oxides and hydroxides of Fe and Mn are important scavengers for REEs (Aubert et al., 2001; Karadağ et al., 2009; Abedini and Calagari, 2013a; Yusoff et al., 2013). In this study, for determination of potential host minerals for REEs in the ores at Kanigorgeh, attempts have been made to calculate Pearson correlation coefficients between REEs and major and minor elements (Table 6). The negative correlation between Si and lanthanides (r = –0.25 to –0.39) and positive but weak correlation between Al and lanthanides (r = 0.16 to 0.30) show that clay minerals are not the likely hosts for REEs in the profile. Negative and weak correlations between Fe and most of the REEs (r = –0.03 to –0.12) point to the weak role of Fe-bearing minerals for concentrations of REEs in the residual profile. The negative correlation coefficients between P and REEs (r = –0.15 to –0.44) indicates that the P-bearing minerals did not play any role for concentration of lanthanides. Although De Carlo et al. (1998), Bau (1999), and Ohta and Kawabe (2001) reported that there is a close relationship between Ce and Fe and Mn in the weathered systems, Ce at Kanigorgeh displays a good correlation only with Mn (r = 0.85), indicating the role of Mn-oxides in fixation of this element. This high correlation coefficient also shows that, analogous to Ce, the variation in redox potential is a key factor for distribution of Mn in this profile (Ma et al., 2007). The existence of a strong and positive correlation between Mn and REE (r = 0.71 to 0.98) may also indicate the effective role of Mn-oxides in concentration of REEs at Kanigorgeh. Mn-oxides also have good and positive correlations with Ni, Zn, Tl, and Pb (r = 0.84–0.94), which may reflect their significant role in fixation of these elements in the system (Ndjigui et al., 2013). The positive but weak correlations between Ti and all REEs (r = 0.21–0.32) may point to the fact that, despite the existence of noticeable quantities of TiO_2 in the form of rutile and anatase in the ores, these 2 Ti-bearing mineral phases did not play a drastic role in the concentration and distribution of REEs in the ores at Kanigorgeh.

6. Conclusions

The most important results obtained from these mineralogical and geochemical studies of the Ti-rich karst bauxite ores in the 10-m-thick Permian bauxite horizon at Kanigorgeh are as follows:

1) The studied ores contain ooidic, pisoidic, nodular, and collomorphic-fluidal textures. Diaspore along with kaolinite, boehmite, smectite, illite, rutile, hematite, goethite, chlorite, quartz, and plagioclase are rock-forming minerals in the ores at Kanigorgeh.

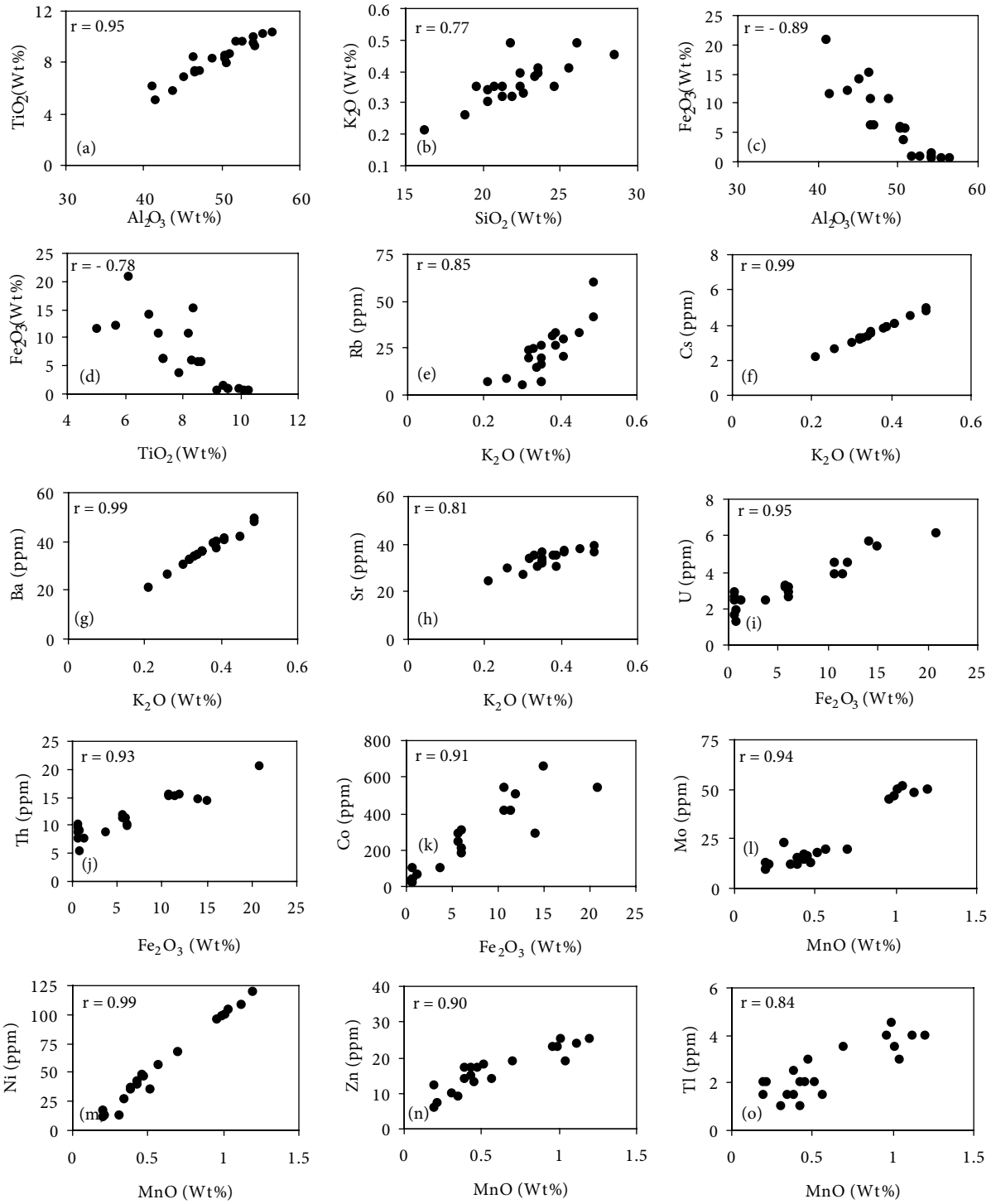

Figure 8. Binary diagrams showing the correlations between **(a)** Al_2O_3 and TiO_2, **(b)** SiO_2 and K_2O, **(c)** Al_2O_3 and Fe_2O_3, **(d)** Fe_2O_3 and TiO_2, **(e)** K_2O and Rb, **(f)** K_2O and Cs, **(g)** K_2O and Ba, **(h)** K_2O and Sr, **(i)** Fe_2O_3 and U, **(j)** Fe_2O_3 and Th, **(k)** Fe_2O_3 and Co, **(l)** MnO and Mo, **(m)** MnO and Ni, **(n)** MnO and Zn, and **(o)** MnO and Tl in the studied bauxite ores.

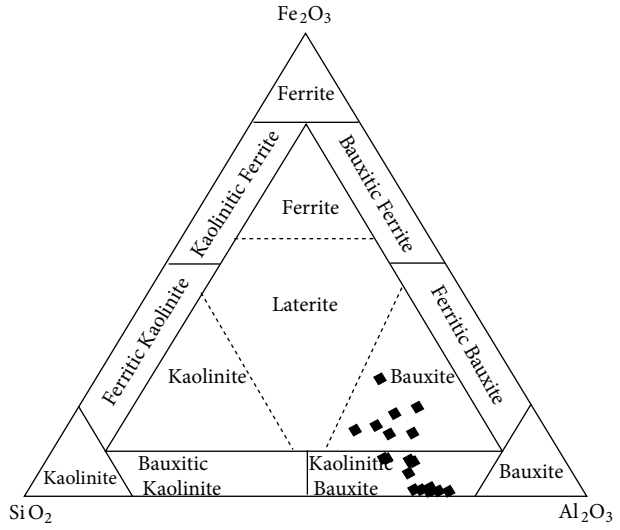

Figure 9. Ternary plot of SiO_2–Al_2O_3–Fe_2O_3 (Aleva, 1994) for the bauxite ores. The Kanigorgeh data points are plotted both in bauxite and kaolinitic bauxite domains.

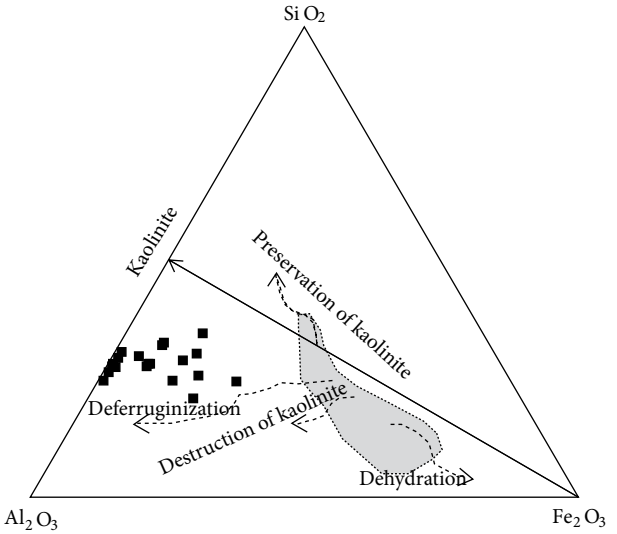

Figure 11. Ternary plot for probable geochemical paths according to Beauvais (1991) indicating various trends followed during the process of bauxitization depending upon whether quartz is present or absent in the soft microgranular matrix. The shaded portion shows data of ferruginous cuirasses (Tardy, 1997). As shown on this plot, the Kanigorgeh bauxite ores resulted from deferruginization processes.

2) The studied profile (~10 m thick) is divided into 2 parts by a redox boundary at a depth of 6.5 m. The upper part is a leached zone, in which the ores have positive Ce anomalies and low values of REEs (174–548 ppm). In comparison, the lower part of the profile is an accumulation zone and separated from the upper part by the negative Ce anomalies and high REE values (541–1250 ppm). The positions of these 2 zones indicate that leaching and fixation were 2 important mechanisms principally controlling the distribution of REEs in the ores.

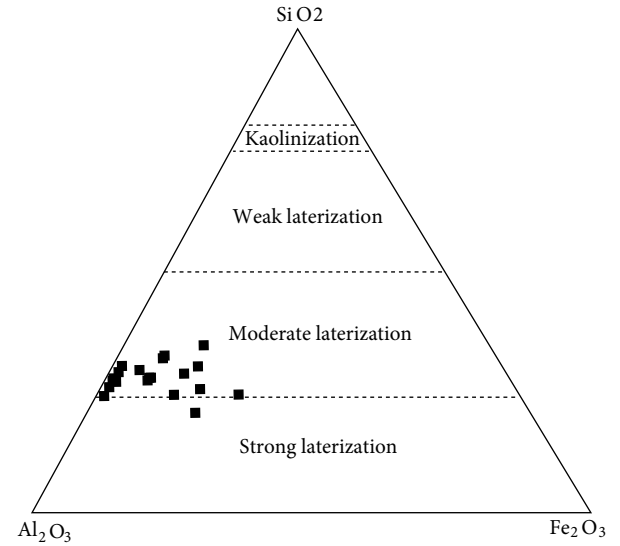

Figure 10. Ternary plot of SiO_2–Al_2O_3–Fe_2O_3 (Schellmann, 1986) for the bauxite ores. The Kanigorgeh data points are plotted principally in moderate laterization field.

3) The positive Ce anomalies in the upper part of the profile point to the fixation of Ce^{4+} under oxidizing conditions in the ores. The negative Ce anomalies in the lower part of the profile reveal that carbonate ligands for complexing with Ce^{4+} were present in considerable quantities in the environment of ore deposition in the horizon.

4) The obtained results showed that the relatively narrow variations of negative Eu anomalies in the profile were controlled chiefly by the degree of feldspar alteration.

5) Incorporation of the results obtained from considerations of variation trends of REEs, LREEs, MREEs, HREEs, and La/Y along with values of La_N/Yb_N, La_N/Sm_N, and Gd_N/Yb_N in the ores reveal that the degrees of leaching, fractionation, and concentration of REE are functioned by factors such as variation in chemistry (Eh, pH) of ore-forming solutions, degree of accessibility to complexing ligands, differences in stability of REE-bearing primary minerals, function of carbonate bedrocks as an active geochemical barrier, and scavenging by Mn-oxides.

6) Correlation coefficients among elements illustrated that Mn-oxides in this deposit played a prominent role in concentration and fixation of elements such as Mo, Ni, Zn, Tl, and Pb, in addition to REEs.

7) The geochemical processes effective in mobilization, distribution, and enrichment of REEs in the bauxite ores

Table 3. An overview of the mean values of selected major oxides and REEs of the Permian bauxite deposit at Kanigorgeh and some of the world's representative bauxitic-lateritic deposits of well-known origin.

No.	Locations of bauxite/laterite occurrences	Al_2O_3	SiO_2	Fe_2O_3	TiO_2	MnO	∑REE	References
1	Ayrancı (Turkey)	57.70	3.20	23.36	3.13	0.15	618	Yalcin and Ilhan (2013)
2	Antsirable (Madagascar)	56.80	8.19	8.19	1.69	0.12	304	Berger et al. (2014)
3	Deccan Traps (India)	21.39	32.29	37.45	3.14	0.14	140	Babechuk et al. (2014)
4	Naupaktos (Greece)	49.28	10.76	24.56	1.40	0.09	465	Laskou (2003)
5	Smerna (Greece)	49.27	7.64	30.00	1.61	0.03	290	Laskou (2003)
6	Pylos (Greece)	51.11	11.91	21.11	1.76	0.05	205	Laskou (2003)
7	Los Pijiguaos (Venezuela)	49.10	11.26	23.48	3.44	0.06	-	Meyer et al. (2002)
8	Shahindesh (Iran)	32.31	28.19	24.72	2.92	0.06	266.57	Abedini and Calagari (2013c)
9	Menderes Massif (Turkey)	61.12	4.27	23.11	3.02	0.03	-	Aydoğan and Moazzen (2012)
10	Maşatdağı (Turkey)	55.31	11.26	23.48	3.44	0.06	-	Temur (2006)
11	Seydişehir/Konya (Turkey)	48.86	8.06	16.74	2.06	0.01	740.35	Karadağ et al. (2009)
12	Biglar (Iran)	32.29	20.89	25.96	5.61	0.04	245.71	Calagari et al. (2010)
13	Kanigorgeh (Permo-Triassic)	38.62	20.55	22.38	4.72	0.06	510.88	Abedini and Calagari (2013b)
14	Jajarm (Iran)	34.00	27.30	21.60	3.60	0.02	703.70	Esmaeili et al. (2010)
15	Sheikh-Marut (Iran)	21.32	41.11	17.69	3.07	0.29	507.10	Abedini an Calagari (2013a)
16	Apulian (Italy)	39.85	7.96	36.32	5.19	0.16	930.70	Mongelli (1997)
17	Northern Ireland	33.78	21.54	25.03	3.99	0.10	-	Hill et al. (2000)
18	Olmedo (Italy)	52.00	19.84	10.65	2.71	0.02	-	MacLean et al. (1997)
19	Kanigorgeh (Permian)	49.95	22.26	6.69	8.19	0.60	96.78	This study

Table 4. Values of Eu/Eu*, Ce/Ce*, La/Y, REEs, LREEs, MREEs, HREEs, La_N/Yb_N, La_N/Sm_N, and Gd_N/Yb_N for the studied bauxite ores at Kanigorgeh.

	R-1	R-2	R-3	R-4	R-5	R-6	R-7	R-8	R-9	R-10
Eu/Eu*	0.42	0.42	0.60	0.49	0.59	0.54	0.47	0.49	0.54	0.49
Ce/Ce*	2.33	2.25	2.73	1.88	2.98	3.01	2.56	1.89	3.13	1.62
La/Y	1.05	1.13	0.19	0.34	0.47	0.16	1.01	0.38	0.25	0.72
$\sum REE_{La-Lu}$	133.98	104.64	20.86	52.58	101.86	15.41	84.68	52.69	36.20	83.84
$\sum LREE_{La-Nd}$	111.34	91.29	18.43	36.29	96.06	13.56	62.90	36.40	27.25	53.66
$\sum MREE_{Sm-Ho}$	16.95	9.72	1.80	13.66	4.74	1.38	17.64	13.66	7.17	25.53
$\sum HREE_{Er-Lu}$	5.69	3.63	0.63	2.63	1.06	0.47	4.14	2.63	1.78	4.65
La_N/Yb_N	0.67	1.17	1.18	0.64	1.54	1.00	0.85	0.64	0.44	0.54
La_N/Sm_N	1.74	4.56	4.93	1.21	3.22	4.53	2.01	1.21	0.80	0.95
Gd_N/Yb_N	1.54	0.93	0.19	1.54	0.50	0.14	1.91	1.54	0.76	2.88
	R-11	R-12	R-13	R-14	R-15	R-16	R-17	R-18	R-19	R-20
Eu/Eu*	0.57	0.55	0.47	0.65	0.49	0.51	0.42	0.43	0.44	0.52
Ce/Ce*	3.23	2.7	2.06	2.08	0.31	0.61	0.6	0.21	0.24	0.44
La/Y	0.09	0.36	1.15	1.06	6.11	4.58	3.46	4.51	3.71	3.00
$\sum REE_{La-Lu}$	8.91	30.44	96.46	84.41	175.5	200.38	192.17	152.79	151.04	156.93
$\sum LREE_{La-Nd}$	7.63	26.33	74.68	77.01	141.84	167.46	160.23	120.85	120.29	130.19
$\sum MREE_{Sm-Ho}$	0.95	3.28	17.64	5.51	23.95	24.19	24.18	24.18	23.04	19.75
$\sum HREE_{Er-Lu}$	0.33	0.83	4.14	1.89	9.71	8.73	7.76	7.76	7.71	6.99
La_N/Yb_N	0.63	1.06	0.85	1.85	1.39	1.46	1.55	1.55	1.52	1.55
La_N/Sm_N	3.63	2.67	2.02	4.20	5.15	4.29	3.60	3.60	3.82	3.60
Gd_N/Yb_N	1.44	2.45	3.18	1.16	1.21	1.34	1.50	1.50	1.46	1.00

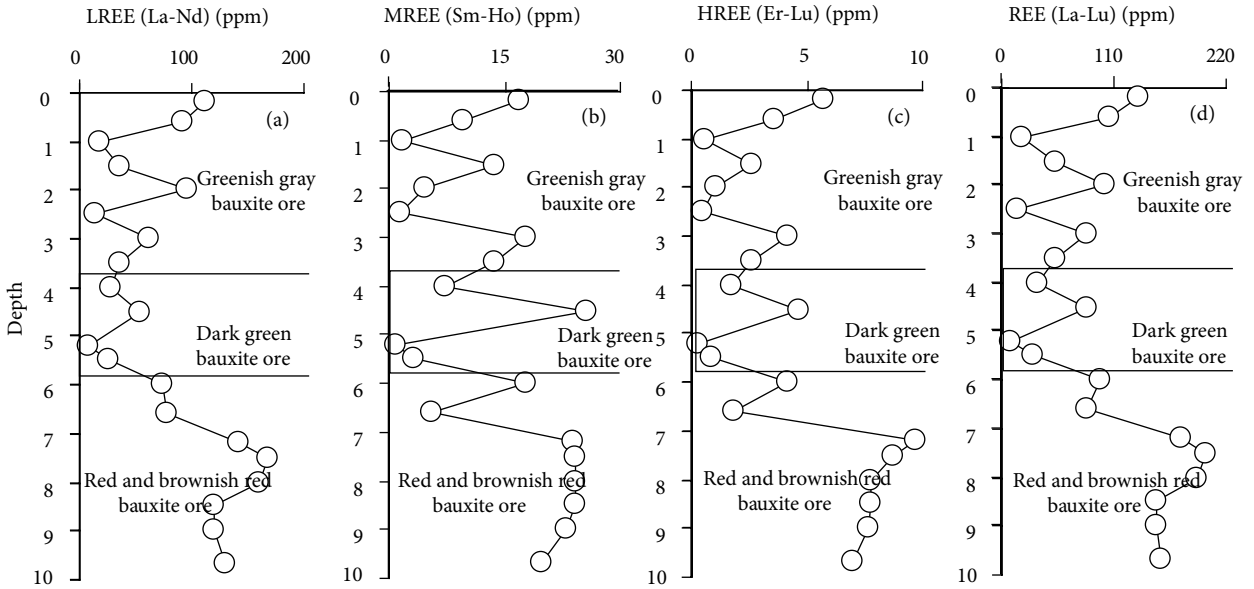

Figure 12. Concentration variations of **(a)** LREEs (La–Nd), **(b)** MREEs (Sm–Ho), **(c)** HREEs (Er–Lu), and **(d)** REEs (La–Lu) in the bauxite ores against depth in the studied profile at Kanigorgeh.

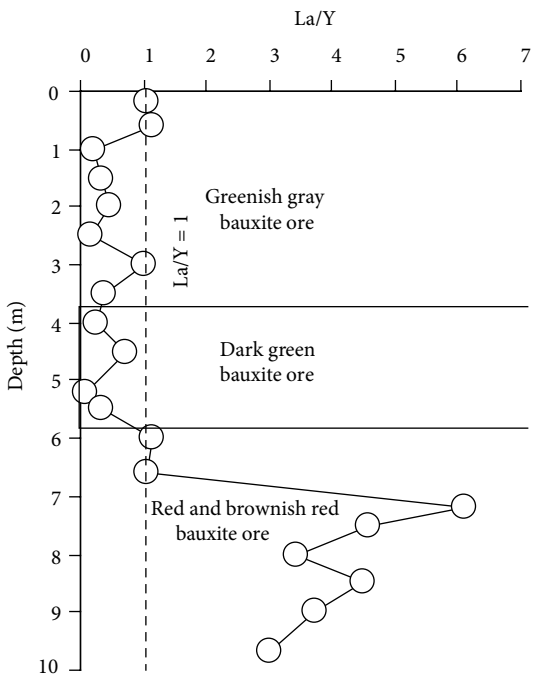

Figure 13. Variation of La/Y values in the bauxite ores against depth in the studied profile at Kanigorgeh.

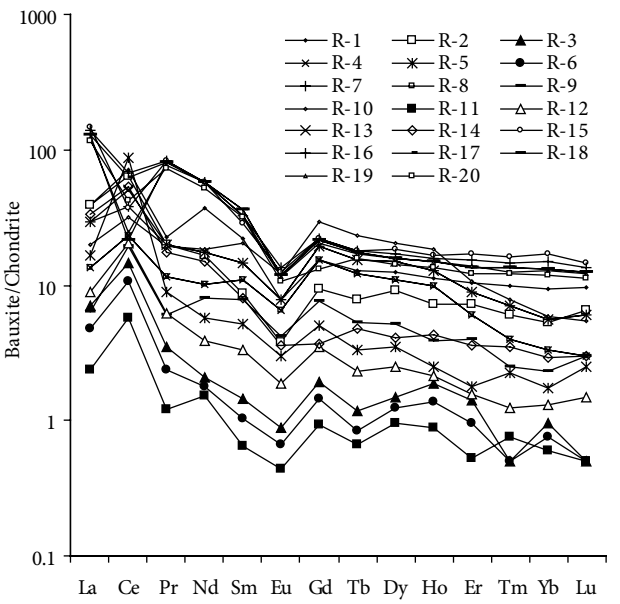

Figure 14. The chondrite-normalized REE patterns of the bauxite ores at Kanigorgeh.

Table 5. Pearson correlation coefficient values among REE in the bauxite ores at Kanigorgeh.

	La	Ce	Pr	Nd	Sm	Eu	Gd	Tb	Dy	Ho	Er	Tm	Yb	Yb
La	1.00													
Ce	0.74	1.00												
Pr	0.99	0.75	1.00											
Nd	0.98	0.75	0.99	1.00										
Sm	0.93	0.76	0.96	0.97	1.00									
Eu	0.82	0.75	0.85	0.87	0.94	1.00								
Gd	0.61	0.57	0.65	0.68	0.81	0.93	1.00							
Tb	0.66	0.62	0.71	0.74	0.85	0.96	0.98	1.00						
Dy	0.68	0.61	0.71	0.73	0.84	0.96	0.98	0.99	1.00					
Ho	0.72	0.65	0.76	0.79	0.88	0.97	0.97	0.99	0.99	1.00				
Er	0.89	0.72	0.92	0.93	0.95	0.97	0.87	0.91	0.92	0.94	1.00			
Tm	0.95	0.75	0.96	0.97	0.97	0.94	0.80	0.85	0.86	0.89	0.98	1.00		
Yb	0.98	0.75	0.98	0.98	0.95	0.90	0.74	0.79	0.80	0.83	0.97	0.99	1.00	
Lu	0.97	0.74	0.97	0.98	0.96	0.90	0.74	0.79	0.81	0.84	0.97	0.99	0.99	1.00

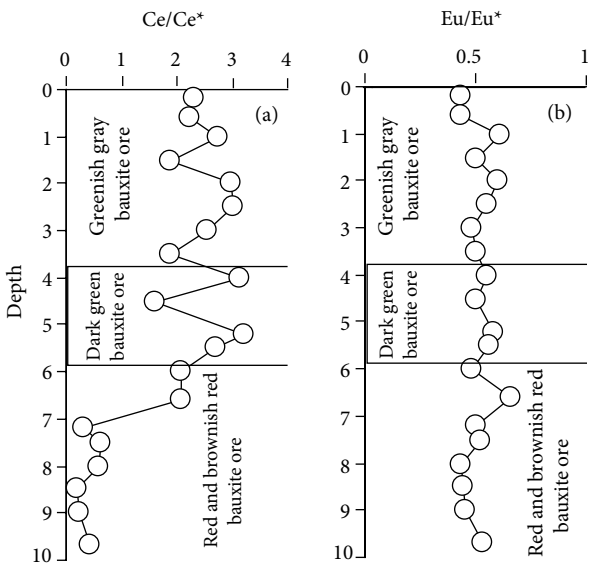

Figure 15. Variation of **(a)** Ce/Ce* and **(b)** Eu/Eu* values in the bauxite ores against depth in the studied profile at Kanigorgeh.

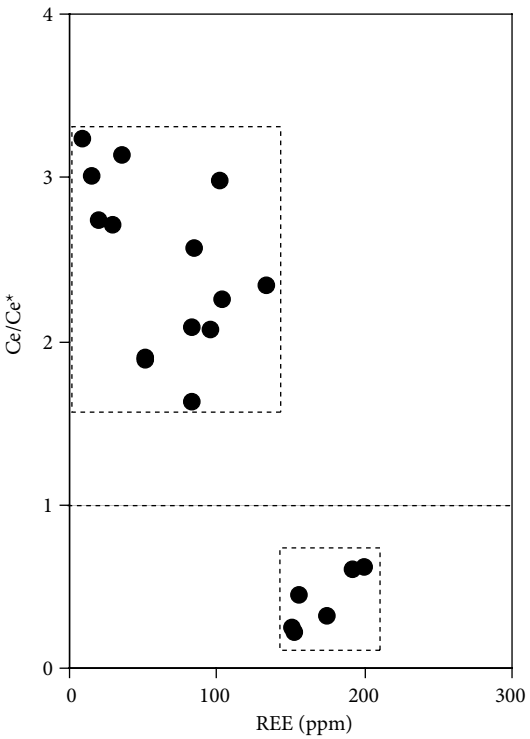

Figure 16. Variation of the total concentration values of REE versus Ce/Ce* in the studied bauxite ores at Kanigorgeh.

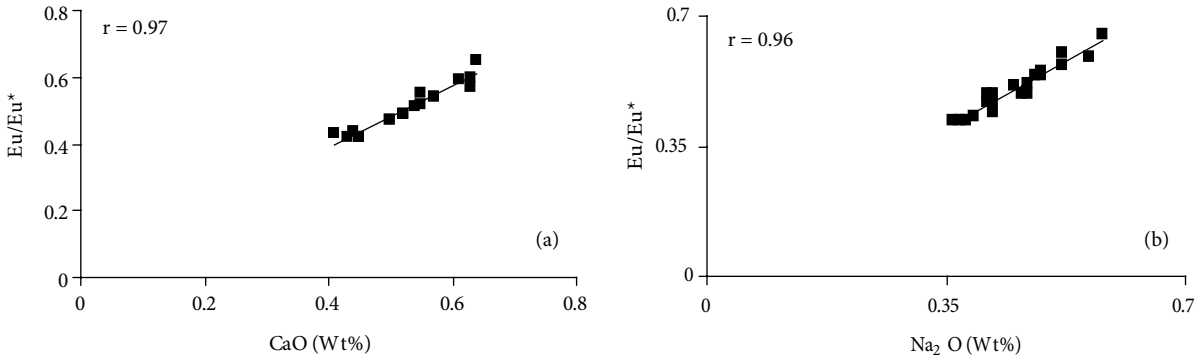

Figure 17. Diagrams featuring the positive correlation between pairs of **(a)** CaO–Eu/Eu* and **(b)** Na_2O–Eu/Eu* for the bauxite ores at Kanigorgeh.

Table 6. Pearson correlation coefficient values among REEs and major and minor elements in the bauxite ores at Kanigorgeh.

	Si	Al	Fe	Ca	Mg	Na	K	Ti	Mn	P
La	–0.26	0.22	–0.10	–0.19	–0.02	–0.07	0.05	0.26	0.96	–0.20
Ce	–0.39	0.28	–0.08	–0.38	–0.18	–0.25	–0.23	0.31	0.85	–0.44
Pr	–0.26	0.25	–0.12	–0.18	0.00	–0.06	0.07	0.27	0.97	–0.18
Nd	–0.27	0.26	–0.13	–0.16	0.02	–0.06	0.08	0.29	0.98	–0.16
Sm	–0.28	0.30	–0.16	–0.16	0.03	–0.08	0.07	0.32	0.97	–0.15
Eu	–0.33	0.20	–0.02	–0.22	–0.06	–0.13	0.02	0.24	0.90	–0.22
Gd	–0.29	0.16	0.00	–0.18	–0.08	–0.09	0.03	0.21	0.71	–0.17
Tb	–0.36	0.22	–0.03	–0.24	–0.11	–0.17	–0.02	0.28	0.76	–0.22
Dy	–0.35	0.19	–0.01	–0.23	–0.12	–0.15	0.00	0.26	0.76	–0.22
Ho	–0.37	0.23	–0.04	–0.25	–0.13	–0.17	–0.02	0.30	0.80	–0.23
Er	–0.31	0.19	–0.03	–0.21	–0.07	–0.11	0.04	0.26	0.93	–0.22
Tm	–0.30	0.20	–0.05	–0.22	–0.06	–0.11	0.03	0.25	0.96	–0.23
Yb	–0.27	0.18	–0.04	–0.20	–0.04	–0.08	0.05	0.23	0.97	–0.21
Lu	–0.25	0.21	–0.09	–0.16	0.00	–0.05	0.08	0.26	0.96	–0.18

at Kanigorgeh are similar to the mineralization of REEs in Thailand and southern China.

Acknowledgments

This work was supported financially by the Research Bureau of Urmia University. We would like to express thanks and gratitude to the authorities of this bureau. Our gratitude is further expressed to, Dr Panagiotis Voudouris and an anonymous reviewer for reviewing the manuscript and making critical comments and valuable suggestions.

References

Abedini A, Calagari AA (2013a). Rare earth elements geochemistry of Sheikh-Marut laterite deposit, NW Mahabad, West-Azarbaidjan province, Iran. Acta Geol Sin-Engl 87: 176–185.

Abedini A, Calagari AA (2013b). Geochemical characteristics of Kanigorgeh ferruginous bauxite horizon, West-Azarbaidjan province, NW Iran. Period Mineral 82: 1–23.

Abedini A, Calagari AA (2013c). Geochemical characteristics of bauxites: the Permian Shahindezh horizon, NW Iran. N J Geol Paläont Abh 270: 301–324.

Alvai-Naeini M, Amidi M, Tatavosian SH, Haghipour A, Boluechi MH, Hajian J, Pelissier G (1976). Geological Map of the Takab-Shahindezh, Scale 1:250,000. Tehran, Iran: Geological Society of Iran.

Aleva GJJ (1994). Laterites: Concepts, Geology, Morphology and Chemistry. Wageningen, the Netherlands: ISIRC.

Aubert D, Stille P, Probst A (2001). REE fractionation during granite weathering and removal by waters and suspended loads: Sr and Nd isotopic evidence. Geochim Cosmochim Ac 65: 387–406.

Aydoğan MS, Moazzen M (2012). Origin and metamorphism of corundum-rich metabauxites at Mt. Ismail in the southern Menderes Massif, SW Turkey. Resour Geol 62: 243–262.

Babechuk MG, Widdowson M, Kamber BS (2014). Quantifying chemical weathering intensity and trace element release from two contrasting basalt profiles, Deccan Traps, India. Chem Geol 363: 56–75.

Bao Z, Zhao Z (2008). Geochemistry of mineralization with exchangeable REY in the weathering crusts of granitic rocks in South China. Ore Geol Rev 33: 519–535.

Bardossy G (1982). Karst Bauxites. Amsterdam, the Netherlands: Elsevier Scientific.

Bardossy GY, Aleva GYY (1990). Lateritic Bauxites. Budapest, Hungary: Akadémiai Kiadó.

Bardossy G, Combes PJ (1999). Karst bauxites: interfingering of deposition and palaeoweathering. In: Thiry M, Simon-Coincon R, editors. Palaeoweathering, Palaeosurface and Related Continental Deposits. New York, NY, USA: John Wiley and Sons, pp. 189–206.

Bau M (1999). Scavenging of dissolved yttrium and rare earths by precipitating iron oxyhydroxide: experimental evidence for Ce oxidation, Y-Ho fractionation, and lanthanide tetrad effect. Geochim Cosmochim Ac 63: 67–77.

Beauvais A (1991). Palaeoclimats et dynamique d'un paysage cuirasee du Centrafreque. Morphologie, petrologie et geochimie. PhD, University of Poitiers, Poitiers, France (in French).

Berger A, Janots E, Gnos E, Frei R, Bernier F (2014). Rare earth element mineralogy and geochemistry in a laterite profile from Madagascar. Appl Geochem 41: 218–228.

Boni M, Reddy SM, Mondillo N, Balassone G, Taylor R (2012). A distant magmatic source for Cretaceous karst bauxites of southern Apennines (Italy), revealed through SHRIMP zircon age dating. Terra Nova 24: 326–332.

Boni M, Rollinson G, Mondillo N, Balassone G, Santoro L (2013). Quantitative mineralogical characterization of karst bauxite deposits in the southern Apennines, Italy. Econ Geol 108: 813–833.

Calagari AA, Abedini A (2007). Geochemical investigations on Permo–Triassic bauxite deposit at Kanisheeteh, east of Bukan, Iran. J Geochem Explor 94: 1–18.

Calagari AA, Kangrani F, Abedini A (2010). Geochemistry of minor, trace and rare earth elements in Biglar Permo-Triassic bauxite deposit, northwest of Abgarm, Ghazvin Province, Iran. J Sci Islamic Repub Iran 21: 225–236.

Chi R, Tian J (2009). Weathered Crust Elution-Deposited Rare Earth Ores. New York, NY, USA: Nova.

Crinci J, Jurkowic I (1990). Rare earth elements in Triassic bauxites of Croatia Yugoslavia. Travaux 19: 239–248.

De Carlo EH, Wen XY, Irving M (1998). The influence of redox reactions on the uptake of dissolved Ce by suspended Fe and Mn oxide particles. Aquat Geochem 3: 357–389.

Efthekhar-Nezad J (1973). Geological map of the Mahabad, Scale 1:250,000. Tehran, Iran: Geological Society of Iran.

Esmaeili D, Rahimpour-Binab H, Esna-Ashari A, Kananian A (2010). Petrography and geochemistry of the Jajarm karst bauxite ore deposit, NE iran: implications for source rock material and ore genesis. Turkish J Earth Sci 19: 267–284.

Gamaletsos P, Godelitsas A, Mertzimekis TJ, Göttlicher J, Steininger R, Xanthos S, Berndt J, Klemme S, Kuzmin A, Bárdossy G (2011). Thorium partitioning in Greek industrial bauxite investigated by synchrotron radiation and laser-ablation techniques. Nucl Instrum Meth B 269: 3067–3073.

Giorgis I, Bonetto S, Giustetto R, Lawane A, Pantet A, Rossetti P, Thomassin J, Vinai R (2014). The lateritic profile of Balkouin, Burkina Faso: geochemistry, mineralogy and genesis. J African Earth Sci 90: 31–48.

Gu J, Hunang Z, Fan H, Jin Z, Yan Z, Zhang J (2013). Mineralogy, geochemistry, and genesis of lateritic bauxite deposits in the Wuchuan–Zhengan–Daozhen area, Northern Guizhou Province, China. J Geochem Explor 130: 44–59.

Hanilçi N (2013). Geological and geochemical evolution of the Bolkardaği bauxite deposits, Karaman, Turkey: transformation from shale to bauxite. J Geochem Explor 133: 118–137.

Hatipoğlu M (2011). Al (Fe, Ti, Si) mobility and secondary mineralization implications: a case study of the karst unconformity diasporite-type bauxite horizons in Milas (Muğla), Turkey. J African Earth Sci 60: 175–195.

Hatipoğlu M, Türk N, Chamberlain SC, Akgün AM (2010). Gem–quality transparent diaspore (zultanite) in bauxite deposits of the İlbir Mountains, Menderes Massif, SW Turkey. Miner Deposita 45, 201–205.

Hill IG, Worden RHG, Meighan IG (2000). Geochemical evolution of a paleolaterite: the interbasaltic formation, Northern Ireland. Chem Geol 166: 65–84.

Kamineni DC, Efthekhar–Nezad J (1977). Mineralogy of the Permian laterite of Northwestern Iran. Tscher Miner Petrog 24: 95–204.

Karadağ M, Küpeli S, Arýk F, Ayhan A, Zedef V, Döyen A (2009). Rare earth element (REE) geochemistry and genetic implications of the Mortaş bauxite deposit (Seydişehir/Konya–Southern Turkey). Chemie Erde-Geochem 69: 143–159.

Laskou M, Economou-Eliopoulos M (2007). The role of microorganisms on the mineralogical and geochemical characteristics of the Parnassos-Ghiona bauxite deposits, Greece. J Geochem Explor 93: 67–77.

Laskou M, Economou-Eliopoulos M (2013). Bio-mineralization and potential biogeochemical processes in bauxite deposits: genetic and ore quality significance. Miner Petrol 107: 471–486.

Laskou MD (2003). Geochemical and mineralogical characteristics of the bauxite deposits of western Greece. In: Eliopoulos, editor. Mineral Exploration and Sustainable Development, 7th Biennial SGA Meeting. Athens, Greece: SGA, pp. 93–96.

Li Z, Din J, Xu J, Liao C, Yin F, Lǔ T, Cheng C, Li J (2013). Discovery of the REE minerals in the Wulong-Nanchuan bauxite deposits, Chongqing, China: insights on conditions of formation and processes. J Geochem Explor 133: 88–102.

Liu X, Wang Q, Deng J, Zhang Q, Sun S, Meng J (2010). Mineralogical and geochemical investigations of the Dajia Salento-type bauxite deposits, western Guangxi, China. J Geochem Explor 105: 137–152.

Liu X, Wang Q, Feng Y, Li Z, Cai S (2013). Genesis of the Guangou karstic bauxite deposit in western Henan, China. Ore Geol Rev 55: 162–175.

Liu X, Wang Q, Zhang Q, Feng Y, Cai S (2012). Mineralogical characteristics of the superlarge Quaternary bauxite deposits in Jingxi and Debao counties, western Guangxi, China. J Asian Earth Sci 52: 53–62.

Ma J, Wei G, Xu Y, Long W, Sun W (2007). Mobilization and redistribution of major and trace elements during extreme weathering of basalt in Hainan Island, South China. Geochim Cosmochim Ac 71: 3223–3237.

MacLean WH, Bonavia FF, Sanna G (1997). Argillite debris converted to bauxite during karst weathering: evidence from immobile element geochemistry at the Olmedo deposit, Sardinia. Miner Deposita 32: 607–616.

Mameli P, Mongelli G, Oggiano G, Dinelli E (2007). Geological, geochemical and mineralogical features of some bauxite deposits from Nurra (western Sardinia, Italy): insights on conditions of formation and parental affinity. Int J Earth Sci 96: 887–902.

Meshram RR, Randive KR (2011). Geochemical study of laterites of the Jamnagar district, Gujarat, India: implications on parent rock, mineralogy and tectonics. J Asian Earth Sci 42: 1271–1287.

Meyer FM, Happel U, Hausberg J, Wiechowski A (2002). The geometry and anatomy of the Pijigaos bauxite deposit, Venezuela. Ore Geol Rev 20: 27–54.

Mondillo N, Balassone G, Boni M, Rollinson GG (2011). Karst bauxites in the Campania Apennines (southern Italy): a new approach. Period Mineral 80: 407–432.

Mongelli G (1997). Ce-anomalies in the textural components of Upper Cretaceous karst bauxites from the Apulian carbonate platform (southern Italy). Chem Geol 140: 69–79.

Mongelli G, Boni M, Buccione R, Sinisi R (2014). Geochemistry of the Apulian karst bauxites (southern Italy): chemical fractionation and parental affinities. Ore Geol Rev 63: 9–21.

Mordberg LE (1996). Geochemistry of race elements in Paleozoic bauxite profiles in Northern Russia. J Geochem Explor 57: 187–199.

Nabavi M (1976). An Introduction to the Geology of Iran. Tehran, Iran: Geological Survey of Iran Publication (in Persian).

Ndjigui PD, Badinane MFB, Nyeck B, Nandjip HPK, Bilong P (2013). Mineralogical and geochemical features of the coarse saprolite developed on orthogneiss in the SW of Yaoundé, South Cameroon. J African Earth Sci 79: 125–142.

Ohta A, Kawabe I (2001). REE(III) adsorption into Mn dioxide (α - MnO_2) and Fe oxyhyroxide: Ce(III) oxidation by α–MnO_2. Geochim Cosmochim Ac 65: 695–703.

Özlü N (1983). Trace element contents of karst bauxites and their parent rocks in the Mediterranean belt. Miner Deposita 18: 469–476.

Öztürk H, Hein RJ Hanilçi N (2002). Genesis of the Doğankuzu and Mortaş, bauxite deposits, Taurides, Turkey: separation of Al, Fe and Mn and implications for passive margin metallogeny. Econ Geol 97: 1063–1077.

Rudnick RL, Gao S (2004). Composition of the Continental Crust. In: Holland H, Turekian K, editors. Treatise on Geochemistry. 2nd ed. Amsterdam, the Netherlands: Elsevier, pp. 1–64.

Sanematsu K, Kon Y, Imai A, Watanabe K, Watanabe Y (2013). Geochemical and mineralogical characteristics of ion-adsorption type REE mineralization in Phuket, Thailand. Miner Deposita 48: 437–451.

Schellmann W (1986). On the geochemistry of laterites. Chemie Erde 45: 39–42.

Tardy Y (1997). Petrology of Laterites and Tropical Solis. Oxford, UK: IBH Publishing Co. Pvt. Ltd.

Taylor Y, McLennan SM (1985). The Continental Crust: Its Composition and Evolution. 1st ed. Oxford, UK: Blackwell.

Temur S (2006). A geochemical approach to parent rocks of the Maşatdağı diasporic bauxite, Alanya, Antalya, southern Turkey. Geochem Int 44: 941–952.

Temur S, Kansun G (2006). Geology and petrography of the Masatdagi diasporic bauxites, Alanya, Antalya, Turkey. J Asian Earth Sci 27: 512–522.

Temur S, Orhan H, Kurt H (2005). Mass and volume change calculations of Masatdagi (Alanya-Antalya) bauxites from southern Turkey. Geochem Int 43: 202–210.

Wang Q, Liu X, Yan C, Cai S, Li Z, Wang Y, Zhao J, Li G (2012). Mineralogical and geochemical studies of boron-rich bauxite ore deposits in the Songqi region, SW Henan, China. Ore Geol Rev 48: 258–270.

Wang X, Jiao Y, Du Y, Ling W, Wu L, Cui T, Zhou Q, Jin Z, Lei Z, Weng S (2013). REE mobility and Ce anomaly in bauxite deposit of WZD area, Northern Guizhou, China. J Geochem Explor 133: 103–117.

Wei X, Ji H, Li D, Zhang F, Wang S (2013). Material source analysis and element geochemical research about two types of representative bauxite deposits and terra rossa in western Guangxi, southern China. J Geochem Explor 133: 68–87.

Wei X, Ji H, Wang S, Chu H, Song C (2014). The formation of representative lateritic weathering covers in south-central Guangxi (southern China). Catena 118: 55–72.

Yalcin MG, Ilhan S (2008). Major and trace element geochemistry of terra rossa soil in the Kucukkoras Region, Karaman, Turkey. Geochem Int 46: 1038–1054.

Yalcin MG, Ilhan S (2013). Major and trace element geochemistry of bauxites: Ayranci, Karaman, Central Bolkardag, Turkey. Asian J Chem 25: 2893–2904.

Yusoff, ZM, Ngwenya BT, Parsons I (2013). Mobility and fractionation of REEs during deep weathering of geochemically contrasting granites in a tropical setting, Malaysia. Chem Geol 349–350: 71–86.

Zhang Z, Zhou L, Li Y, Wu C, Zheng C (2013). The "coal–bauxite–iron" structure in the ore-bearing rock series as a prospecting indicator for southeastern Guizhou bauxite mines. Ore Geol Rev 53: 145–158.